Measurements for inverse estimation of anisotropic porous materials

Measurements for inverse estimation of anisotropic porous materials

A.L. van Velsen - 0656531

DC 2014.002

Internship

Supervisor: prof. dr. Ines Lopez Arteaga
Supervisor: Christophe van der Kelen

KTH Royal Institute of Technology
Department of aeronautical and vehicle engineering
Eindhoven University of Technology
Department of Mechanical Engineering
Dynamics and Control

Stockholm, January 6, 2014

Summary

Due to the manufacturing process of porous materials, the geometry of the cells of the material differ in rise and injection directions. This introduces an anisotropy in the material. In this report, the measurement methods are given which are used to determine the anisotropic acoustical properties of porous materials. Three different measurements are described. The first measurement is to determine the anisotropic flow resistivity tensor, this property describes the resistivity of a sound pressure wave undergoes by traveling through a porous material. The second and third measurement are together used to determine the stiffness matrix, which gives the stress-strain relationship. The dynamic measurements are used to determine the anelastic moduli and the static measurements are used to determine the elastic moduli. The three measurements are performed on nine cubic samples of melamine foam. The data from the flow resistivity measurement is post-processed with inverse estimation, which gives the anisotropic flow resistivity tensor. The eigenvalue decompositions of the flow resistivity tensor is analyzed and shows that the flow resistivity varies in the principal directions. The stiffness matrix is not determined with inverse estimation yet, but the data from the two measurements is analyzed. From the dynamic measurements it can be seen that the samples do show anisotropic material deformation. The data from the static measurement do not show anisotropic behavior directly.

Contents

Chapter 1

Introduction

Porous materials can be found in different applications. In this report, we are interested in the application in the field of acoustics. Porous materials are often used as sound and vibration absorbers in cars, trains and aircrafts. To be able to make optimal use of the acoustic properties of porous materials, experimental data is needed. The properties of the materials are used in simulations for, for example, single and multiple layer applications. Furthermore, the data can be used in numerical simulation models describing the anisotropic material properties.

The goal of the internship is to perform measurements to gather new data. There are three different measurements. One measurement is used to measure the flow resistivity of a sample. The other two measurements are used to determine the elastic and anelastic moduli of the material. These last two measurements are combined to determine the stiffness matrix of a sample. Furthermore, manuals for the measurements are written, such that measurements can be done for other materials and the same way as in described in this report.

Outline of the report
In Chapter 2, an introduction to the basics about porous materials are given. In Chapter 3, the measurement to determine the flow resistivity tensor is described. In Chapter 4, the dynamic measurement which is used for determining the anelastic part of the stiffness matrix is described. And, in Chapter 5, the measurements for the elastic part of the stiffness matrix can be found. In Chapter 6, the results of the measurements are presented and discussed. Finally, in Chapter 7, the conclusions and recommendations are given.

During the internship, measurements are performed on the material melamine. The measurement manuals are applicable for other porous materials as well. Because of the length of the manuals, these are not included in this report.

Chapter 2

Porous materials

In this chapter, an introduction to porous materials is given. Furthermore, it is explained why it is important to determine the anisotropic properties, instead of the isotropic properties, of porous materials and which material is used for the measurements.

2.1 Porosity

A porous material consists of, at least, two phases: a solid and a fluid. The solid forms a structure of cells, open or closed, that contain the fluid. Porous materials are characterized by its porosity. The porosity, indicated with ϕ, is equal to the ratio between the volume of air in the cavities of a material, V_{air}, and the total volume of the porous material, V_{total} [5]:

$$\phi = \frac{V_{air}}{V_{total}}. \tag{2.1}$$

2.2 Sound absorbance

A porous material is a good sound absorber because of its inner structure. When a sound wave passes through a material, it is reflected by the inner walls of the material. When the sound wave changes direction, some of its energy is absorbed by conversion to heat [6]. Because the material is like a maze, the sound waves travel a large distance before it leaves the absorbing material and the energy of the wave is decreased.

2.3 Anisotropy

The manufacturing process has a high influence on the bulk properties, i.e. density, elastic moduli and damping moduli, of a porous material [6]. Due to gravity effects during the manufacturing process, the material properties differ in the principal directions of the material, and thus are anisotropic. Polymer foams are made by mixing the polymer, a hardener and a

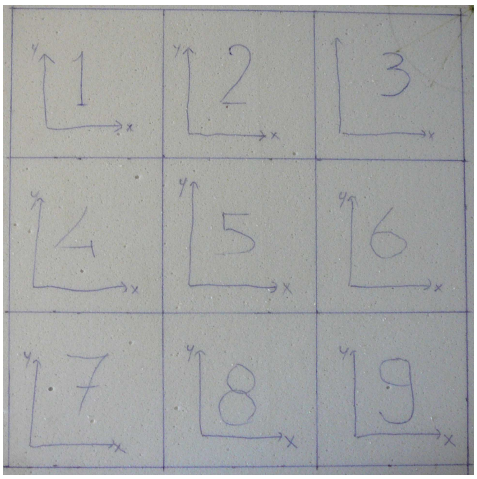

Figure 2.1: The material block before it is cut in 9 samples

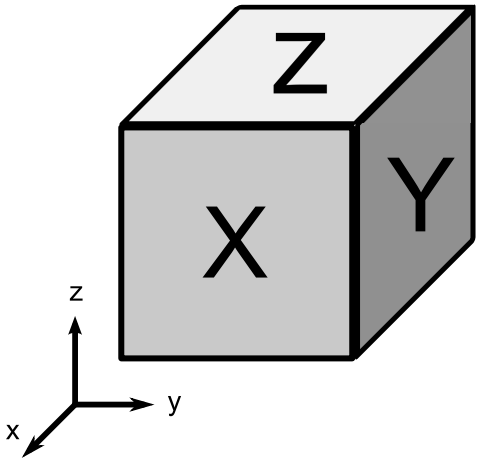

Figure 2.2: The assigned coordinate system, with the Z plane, the top surface of the material

foaming agent into a mall. The material then rises, which results in elongated cells in the rise direction [8]. The measurements described in this report are used to determine the anisotropic properties of porous materials.

2.4 Melamine foam

Melamine is a very light foam with a porosity of approximately 0.99. It is an open-cell foam, which means that the solid material is contained in the cell edges only and the cells are connected through open faces [5]. Melamine has good sound-absorbing and thermal insulation properties [2]. In Figure 2.1, the uncut material, from which the nine samples are taken, is shown. The samples that are cubic with dimensions $100 \times 100 \times 100$ mm. The assigned coordinates that are used in during the measurements and in this report are shown in Figure 2.2.

Chapter 3

Flow resistivity

In this chapter the measurements to determine the anisotropic flow resistivity tensor of a porous material is described.

3.1 Theory

The flow resistivity indicates how much a material resists to the flow of a fluid through the material [7]. To determine the flow resistivity of a porous material, first the flow through the sample must be modeled. The classical model for porous absorbers is based on modeling the absorbent as an homogeneous fluid with viscous damping [7]. The sound field in the porous material can be described by the relation between pressure and particle velocity. This is shown in the following equation of motion, in one dimension and written in the complex form:

$$\rho_0 i\omega \mathbf{u}_x + \frac{\partial \mathbf{p}}{\partial x} + \sigma \mathbf{u}_x = 0 \tag{3.1}$$

with $\mathbf{p}$, a pressure, $\mathbf{u}_x$ the flow rate and σ, the flow resistivity. If we assume that the material is homogenous and isotropic absorbent, then the flow resistivity is given by

$$\sigma = -\frac{\Delta p}{V \cdot t} \tag{3.2}$$

where Δp is the pressure drop over the sample, t is the thickness of the sample and V equals the mean flow of air per unit area of the material. Because porous materials are, as described in Section 2.3, anisotropic due to their manufacturing process, the flow resistance should be specified for each direction, as assigned in Figure 2.2, of the material: σ_x, σ_y and σ_z.

For 3D, the flow resistivity can de described using Darcy's law [4]:

$$\begin{bmatrix} \frac{\partial p}{\partial x} \\ \frac{\partial p}{\partial y} \\ \frac{\partial p}{\partial z} \end{bmatrix} = \begin{bmatrix} \sigma_{xx} & \sigma_{xy} & \sigma_{xz} \\ & \sigma_{yy} & \sigma_{yz} \\ sym & & \sigma_{zz} \end{bmatrix} \begin{bmatrix} u_x \\ u_y \\ u_z \end{bmatrix} \tag{3.3}$$

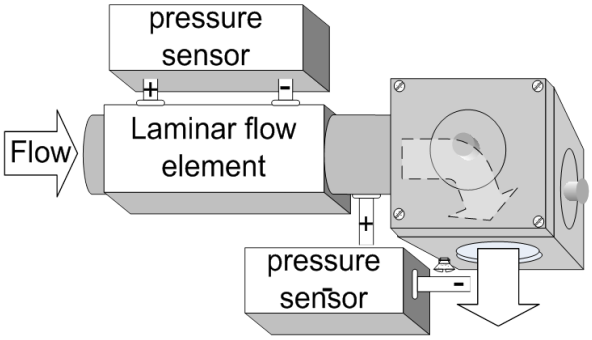

Figure 3.1: Schematic representation of the measurement setup, [6]

3.1.1 Anisotropy and flow resistivity

The rise and injection-flow direction influence the geometry and orientation of the cells [6]. This results in a non-homogenous over the material. It is shown in [4] that the flow resistivity is significantly higher in the rise direction of melamine foam compared to the direction perpendicular to the rise direction. So, it can be said that it is important to measure the anisotropic flow resistivity tensor to describe the material behavior correctly.

3.2 Measurement methodology

To determine the flow resistivity of a sample, both the mean flow through the sample and the pressure difference over a sample are measured. The setup consists of two pressure sensors, one to measure the pressure drop over the sample, and one to measure the pressure drop over a laminair flow element. This laminair flow element is a calibrated device that can be used for determining the velocity from the measured pressure drop. The mean velocity, V is determined from the pressure drop over a calibrated laminar flow element. It can be determined with the following equation. This equation can be found in the calibration file of the laminair flow element.

$$V = B \times \Delta P + C \times \Delta P^2 \tag{3.4}$$

With B and C calibration coefficients and ΔP a pressure difference measured over the laminair flow element.

Furthermore, it is possible to set the air flow speed. To stay in the laminair region in order to prevent non-linear responses the flow rate must be in the range of 0.5 - 4 mm/s, as prescribed in the International Standard ISO 9053 [1]. The setup is shown in Figure 3.1.

The holder that is designed for measuring the anisotropic flow resistivity tensor of a cubic sample is shown in Figure 3.2. The holder has an hole in each side which can be closed with special plugs. By changing the plugs, the outlet face of the sample is changed. Thus, from one inlet, which is mounted onto the air outlet, the pressure drop to all outlets can be measured. By dismounting the holder from the setup, the inlet face can be changed and the pressure drop to all outlets can be measured. A picture of the holder is shown in Figure 3.3.

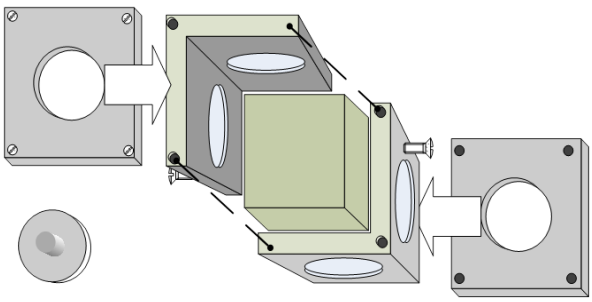

Figure 3.2: Assembling the holder, [6]

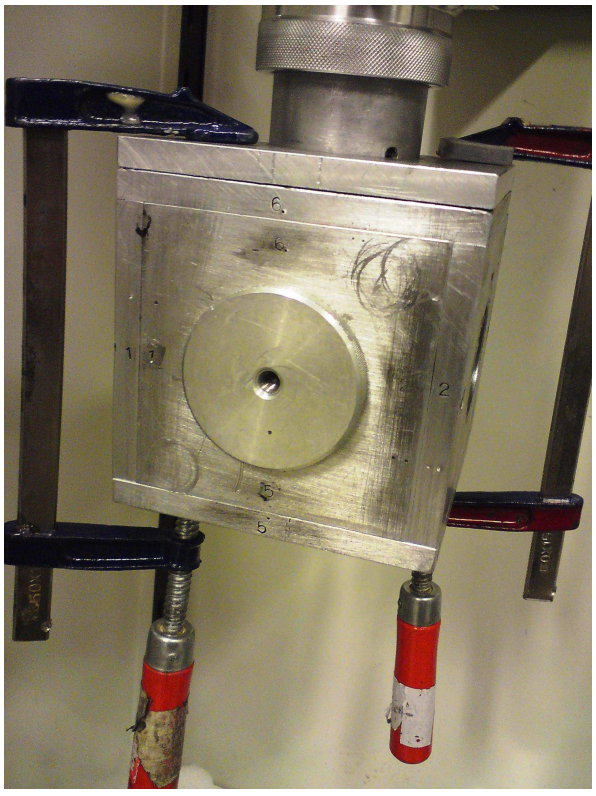

Figure 3.3: The holder mounted with clamps onto the setup.

When all in-outlet combinations are measured, $6 \times 5 = 30$ times the pressure drop and velocity are measured. Because a measurement with, for example, inlet: x^-, outlet: z^+ must give the same result as with inlet: z^+, outlet: x^-. This results in two sets of 15 pressure drops over the laminar flow element and over the foam. These two sets must be the same, so the second set is used as validation for the measured pressure differences.

With the same setup, but with a different sample holder, it is also possible to use cylindrical samples with one sample per direction, x, y, z. In comparison with cubic samples this might give incorrect results, because this measurement does not take the anisotropy in account, with a cubic sample all directions can be measured with one sample.

Calibration

Before the actual measurements can be done, both pressure sensors must be calibrated. Before this is done, it is important that all tubes are connected correctly. The *Swema air*, which measures the pressure drop over the laminar flow element, must be connected to the laminar flow element, the output of the sensor without flow should be zero. If this does not hold, the output can be set to zero. The second sensor which measures the pressure drop over the sample is the *furness controls*. The positive inlet of the furness controls is connected to the outlet above the sample holder. The negative inlet is left open, it measures the atmospheric pressure. The furness control should give, with or without flow, no pressure difference when no sample is connected. If this does not hold, the output can be set to zero. The connection of the sensors is also schematically shown in Figure 1.1.

The measurements are done with al nine samples. The results are presented and discussed in Chapter 6.

Chapter 4

Anelastic moduli

The measurement method to determine the anelastic moduli of porous materials is described in this chapter. First, the theory behind the measurement is discussed. Then, the measurement methodology is described. Some parts of the measurement are explained in more detail, for example some pre-measurement considerations like the measurement time.

4.1 Theory

The dynamical properties of a porous material can be described with the Hooke's law in frequency domain [3]:

$$\sigma_i(\omega) = H_{ij}(\omega)\varepsilon_j(\omega), \quad i,j, = 1,\ldots,6 \tag{4.1}$$

with σ_i containing the components of the stress tensors and ε_i the components of the strain tensors

$$\sigma = \begin{bmatrix}\sigma_{11} & \sigma_{22} & \sigma_{33} & \sigma_{23} & \sigma_{31} & \sigma_{12}\end{bmatrix}^T \tag{4.2}$$

$$\varepsilon = \begin{bmatrix}\varepsilon_{11} & \varepsilon_{22} & \varepsilon_{33} & \varepsilon_{23} & \varepsilon_{31} & \varepsilon_{12}\end{bmatrix}^T \tag{4.3}$$

the matrix H_{ij}, the stiffness matrix, may be written as the sum of an elastic, $H_{ij}^{(0)}$, and an anelastic, $\tilde{H}_{ij}(\omega)$, part [3], given in Equation (4.4). For moduli it is expected that they are higher in the rise direction than in the plane normal to it [8]. The frequency dependent part, the anelastic part, can be determined with the so called *dynamic measurements*. The measurements to determine the elastic part is described in Chapter 4.

$$H_{ij}(\omega) = H_{ij}^{(0)} + \tilde{H}_{ij}(\omega) \tag{4.4}$$

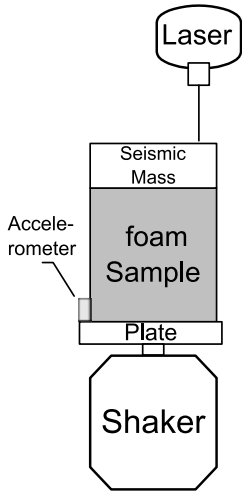

Figure 4.1: Schematic representation of the measurement setup, [6]

4.2 Measurement methodology

The setup consists of a vacuum chamber in which a shaker is positioned. On the shaker a cubic sample, with on top a seismic mass, is mounted. A schematic representation of the setup is shown in Figure 4.1. To determine the viscoelastic moduli of the sample, the transfer function between the acceleration of the bottom plate and the top plate of the sample is measured. The measurements are performed in a vacuum chamber to eliminate the influence of air in the cells [3].

As can be seen in Figure 4.1, an accelerator, which is used to measure acceleration, is mounted on the bottom plate and a laser, which is used to measure velocity, is focussed at different points on the seismic mass. Because we are only interested in acceleration and the laser measures the velocity, multiplication by $i\omega$ is done to determine the acceleration:

$$TF = \frac{V_l}{a} = \frac{i\omega V_l}{a} = \frac{a_l}{a} \tag{4.5}$$

with V_l the velocity measured with the laser, a the acceleration measured with the accelerometer and ω the frequency in [rad/s]. In the following subsections, the most important parts of the measurements are described in detail.

4.2.1 Seismic plates

The seismic masses are used to steer the resonance peak. Plates of, for example, balsa wood and plexiglass are fixed on the sample. Because the sample with the seismic mass can be modeled as a mass-spring-system and the mass of the seismic mass is known, the frequency of the peak can be predicted. The choice of the seismic masses depends on the eigenfrequency of the plate, because the plate resonance of the mass should not influence the measurement, thus the eigenfrequency of the mass must be higher then the frequency range of interest.

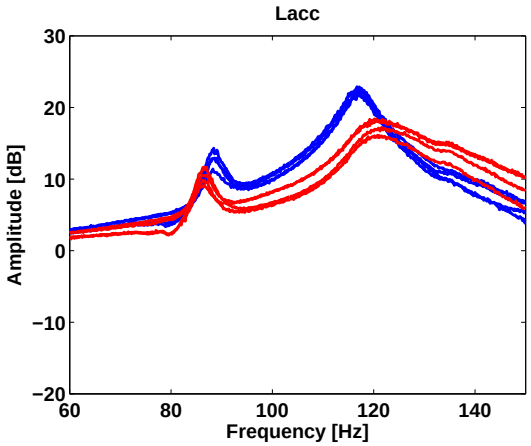

Figure 4.2: The shift of the resonance peak due to change of seismic mass. With in red, the light mass and in blue, the medium mass.

The eigenfrequency depends on the edge conditions, the material properties and the geometry of the plate, can be determined with the following equation [7]:

$$f_{m,n} = \frac{\mu_{m,n}}{2\pi a^2}\sqrt{\frac{Eh^2}{12\rho(1-\upsilon^2)}} \tag{4.6}$$

here, (m,n) are the mode's indices, μ is a constant dependent on the edge conditions, a the length of the edge, h the plate thickness, ρ the plate density, E the elastic modules and υ Poisson's ratio. The plate can be modeled with free-free edge conditions and because the plate is square, the lowest eigenfrequency can be calculated with the lowest mode: $(m,n) = (2,2)$, thus $\mu_{2,2} = 13.5$, this can be found in table 6-8 in [7].

The plates chosen for the measurements are balsa, with dimensions $100 \times 100 \times 10$ mm and have a weight of 12 to 18 grams, and plexiglass, with dimensions $100 \times 100 \times 7.92$ mm and weight approximately 93 gram. Using Equation (4.6), the eigenfrequency of the plexiglass and the balsa plate equal respectively $f_{2,2} = 880$ Hz and $f_{2,2} = 2100$ Hz. These are both higher then the bandwidth, which equals 0 Hz - 500 Hz.

There are three seismic mass combinations:

1. Light: one plate of balsa wood (approx. 15 gram)
2. Medium: two plates of balsa wood (approx. 30 gram)
3. Heavy: one plate of plexiglass (approx. 93 gram)

The measurements are done with a light seismic mass and with a medium mass. An example of two measurements are presented in Figure 4.2. For both situations the measurements of the four corners are shown, four with a light seismic mass in red and four with a medium seismic mass in blue. It can be seen that the frequency response changed due to increase of mass.

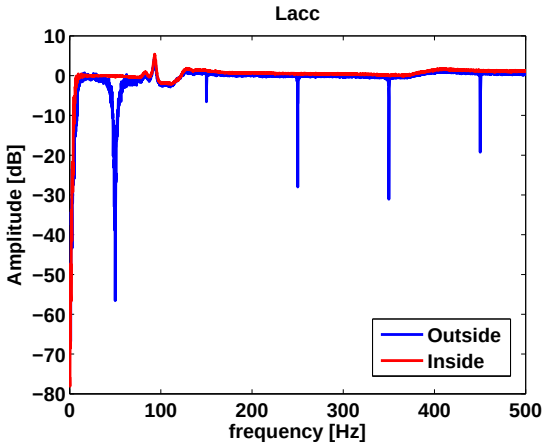

Figure 4.3: Result of grounding the setup by placing the amplifier inside the vacuum chamber

4.2.2 Grounding the setup

In Figure 4.3 the influence of the position of the amplifier is shown. This measurement is performed with the laser pointed at the accelerometer. The laser and the accelerometer should thus give the same output because the measurement is done at the same position on the reference plate. It can be seen that when the amplifier is placed outside the vacuum chamber, the output of the accelerometer differs from the output of the laser, a strong resonance peak is shown at 50 Hz, also its harmonics are visible.

This peak and its harmonics can be explained by the influence of the mains electricity, the alternating current has a frequency of 50 Hz. So, the problem is solved by grounding the setup, which is done by positioning the amplifier of the accelerometer in the vacuum chamber.

4.2.3 Time in vacuum chamber

It is important to be sure that there is no air left in the sample. The air in the cavities causes a decrease in stiffness and thus shifts the resonance frequency, [6]. To determine how long it takes to get all the air out, multiple measurements are be done with a time interval of, for example, 2 hours. This is done for melamine and shown in Figure 4.4. For melamine, a time of 8 hours is used to make sure that no air is left in the sample. So, the pressure in the vacuum chamber must under 30 mbar for 8 hours.

The results of the dynamic measurements are presented and discussed in Chapter 6.

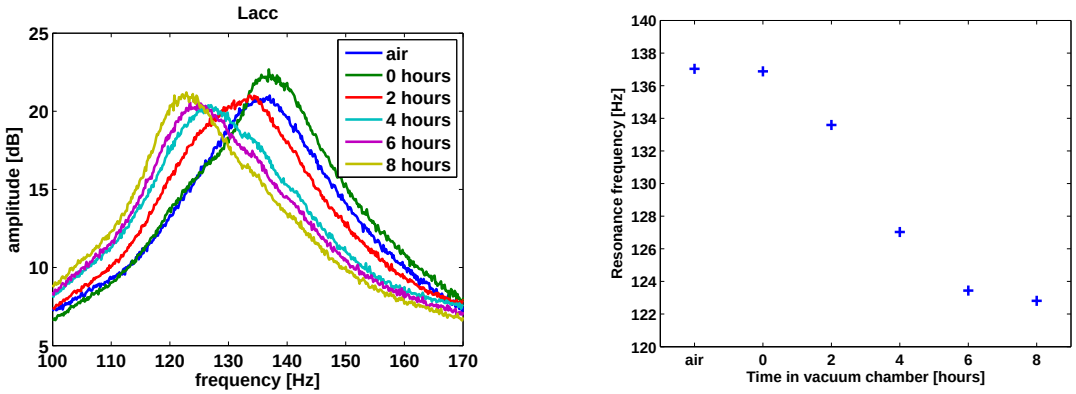

Figure 4.4: Resonance frequency measured at different moments

Chapter 5

Elastic moduli

In this chapter the method to determine the elastic moduli of a porous material is described. Furthermore, the method to measure the applied load is described.

5.1 Theory

The elasticity of a porous material can be described with the Hooke's law, as described in Section 4.1. The frequency independent part, the elastic part $H_{ij}^{(0)}$, can be determined by the so called *static measurement*. Again, the cell orientations cause anisotropy in the material. The linear elastic behavior of the cells is related to the bending of the walls [8].

5.2 Measurement methodology

To determine the static moduli of a porous material, a sample is compressed and the displacement fields in the three principal directions and the applied load are measured. The setup consists of a translating device in which the sample is positioned, as represented in Figure 5.2. A micrometer is mounted on the translating device to apply a compression to the sample with a displacement that can be measured accurate. With the 3D camera setup GOM ARAMIS with image processing, shown in Figure 5.1, the strains resulting from the compression are measured. The size of the sample defines the needed measurement volume as well as the set of lenses that must be used. The lenses and the measuring volume together define the measuring distance to the sample and the base distance of the cameras.

5.2.1 Calibration

When the camera is positioned and aimed, the system must be calibrated. Calibration is needed to make sure that the 3D system has dimensional consistence [9]. The Aramis software guides you through the calibration process with a clear step-by-step instructions. Calibration is done with a calibration plate, more about the calibration plate below.

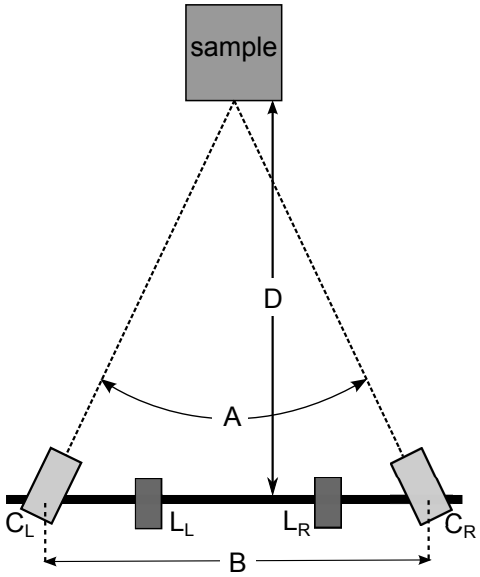

Figure 5.1: The top view of the 3D camera setup. A: Camera angle, B: Base distance, C: Camera left and right, D: measuring distance, L: Lights left and right.

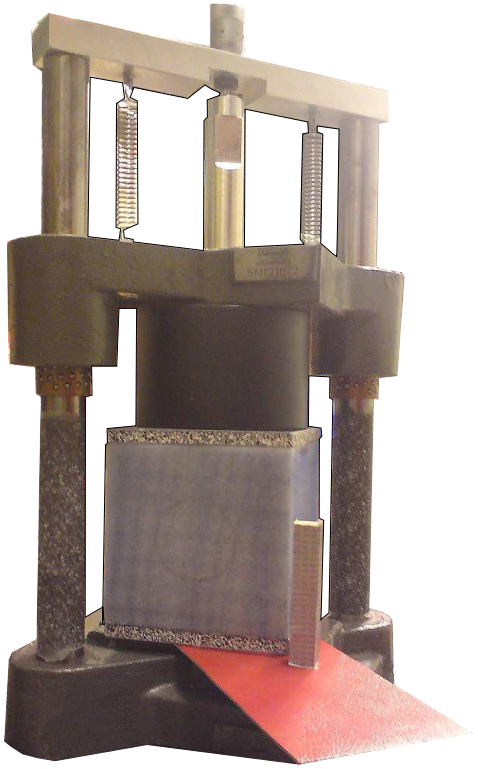

Figure 5.2: The translating device in which a sample is positioned.

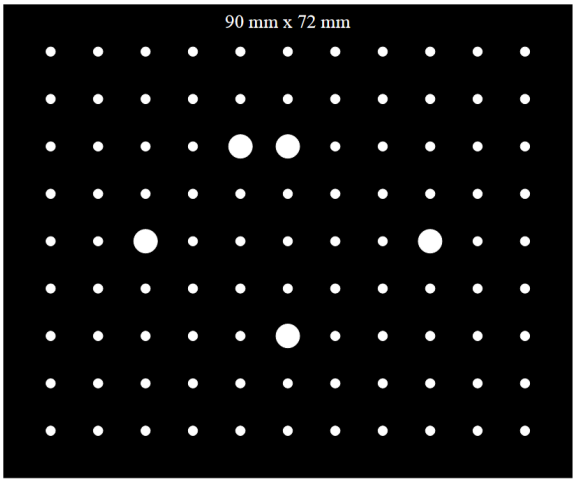

Figure 5.3: An example of a calibration plate, the numbers indicate the measurement volume and the calibration scale.

Calibration plate

The size of the calibration plate depends on the preferred measurement volume and if an one or two camera setup is used. The sample must fit in the measurement volume. In this case, a reference plate of 135 mm $\times$ 108 mm, with a calibration scale, the distance between the two big dots as shown in Figure 5.3, of 81.5 mm. This covers a measurement volume of 135 mm $\times$ 108 mm.

5.2.2 Sample preparation

The ARAMIS software uses recognizable points on the sample to determine the displacements. A sample must have a pattern in order to clearly allocate the pixels in the camera images. [9]. To make the software recognizing points, it is important that the surface of the sample has a high contrast stochastic pattern, an example is shown in Figure 5.4.

Furthermore, the rigid plates, where the sample is fixed in between, also needs a stochastic pattern to make them recognizable for the software. The displacement of these plates can later be used as a reference, because they are known for all measurements.

5.3 Relaxation and load measurement

To measure elastic moduli, it is important to measure the displacement under a constant strain [6]. Therefore, the material should be completely relaxated. From previous experience it is known that this relaxation process takes approximately 8 hours for similar materials. To verify that this holds for the melamine foam, load measurements are done:

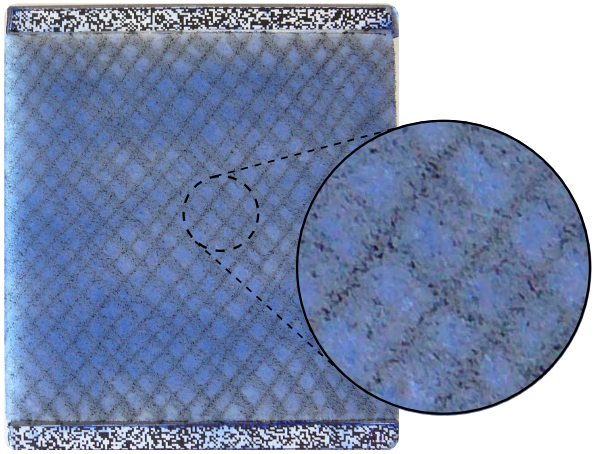

Figure 5.4: An example of a stochastic pattern applied to a sample: the lines are applied with a felt-tip marker.

Compression is slow, with a compression speed of 0.5 mm/s or 1 mm/s, applied to the sample. When the sample is compressed with 2 mm, the relaxation of the sample starts. The load is found to be time dependent during relaxation, shown in Figure 5.5. It can be seen that the load directly decreases and then slowly converges to a constant load, after approximately 6 hours.

5.3.1 Post processing

Post processing of the data is needed to make the data usable. It consists of several steps. First, the data is interpolated and filtered. Then a rotation is applied to align the axis of the data with the axis of the sample. Finally, a movement correction is applied which uses the fact that the bottom plate does not have a displacement. In Figure 5.6, an example of the result of post processing is shown.

The results of the static measurements are presented in Chapter 6.

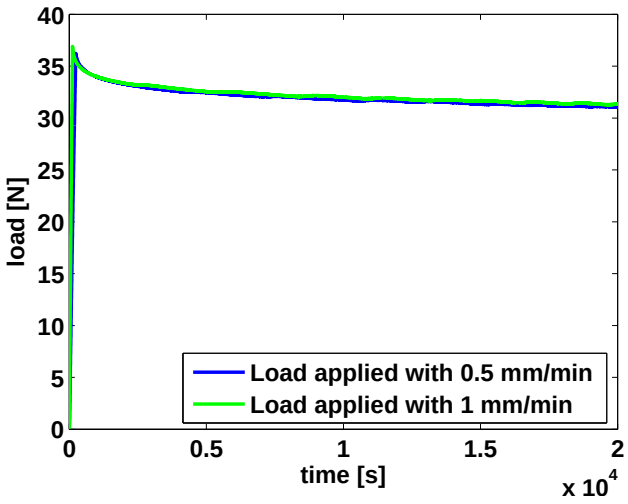

Figure 5.5: Relaxation effect shown with load measurements. The sample is relaxated after 6 hours

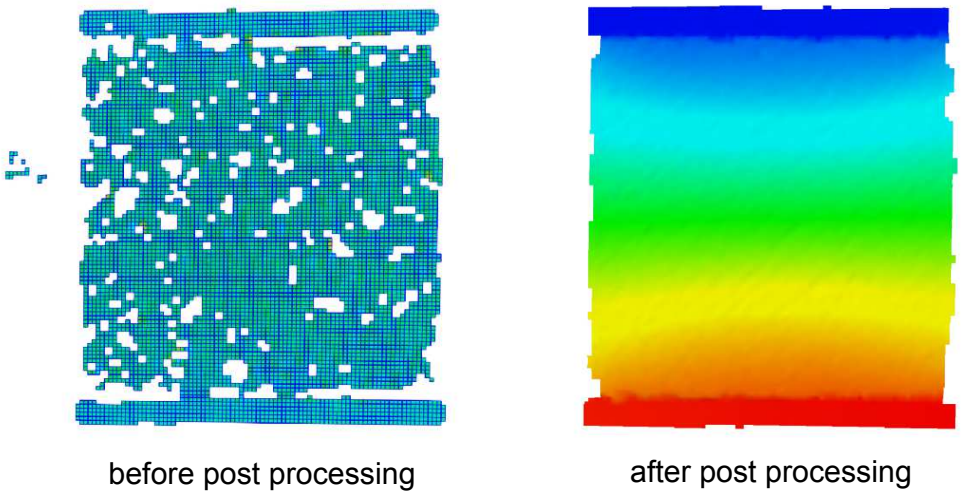

Figure 5.6: Before and after post processing the measured displacement field

Chapter 6

Results

In this chapter the results are presented. First, the inverse estimation will de described briefly. Then, the results of the three measurements are described.

6.1 Inverse estimation

Inverse estimation uses measured data to determine the material properties. Basically, inverse estimation fits a model through measured data. This fitting is done with a minimization process. For all three measurements it uses the error between the data and the model as cost function. For the flow resistivity tensor, the pressure error is minimized. For the anelastic moduli, the error between the frequency responses is minimized. And finally, for the elastic moduli the difference between the displacement fields is minimized.

6.2 Flow resistivity results

The inverse estimation is applied to the data from the flow resistivity measurement for all nine samples. For each sample the anisotropic flow resistivity tensor is determined. Because we are interested in the flow resistivity in the principal directions of the sample, we take a look at the eigenvalue and eigenvector decomposition of the tensor.

The eigenvalue and eigenvector decomposition is applied to the nine flow resistivity tensors, in Appendix A the full decomposition is shown. In Table 6.1 the average flow resistivity for the three principal directions is shown. First of all, the results of sample 6 differ much from the other samples, it might be that something went wrong during the measurements. Therefore, sample 6 is not included in the rest of the discussion of the results. In Table 6.1 it can be seen that in the Z direction the flow resistivity has the highest value. The values for the X and Y direction are lower but do not differ so much.

The direction of the highest flow resistivity is aligned with the rise direction [4], so it can be said that the rise direction corresponds with the Z direction of our samples. Furthermore, these results show that the tested samples are not isotropic with respect to the flow resistivity.

Table 6.1: Averages flow resistivity for the principle directions

direction	Average Flow resistivity	Standard deviation
X	6.465	0.246
Y	6.568	0.234
Z	6.967	0.244

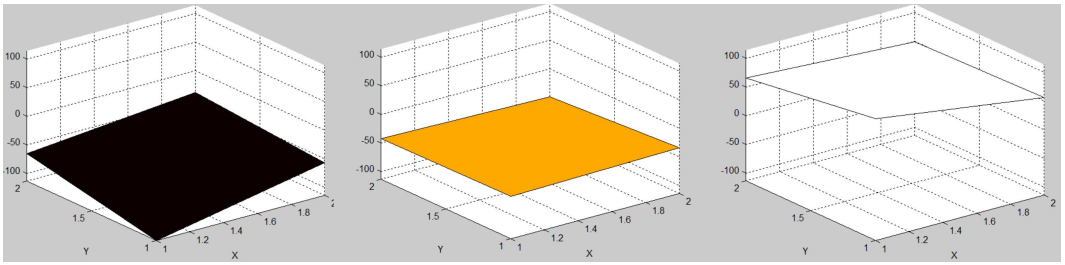

Figure 6.1: Measured displacement relative to the maximum deformation, response at a frequency of 120 Hz

6.3 Dynamic measurements results

The inverse estimation is not jet applied to the dynamic and static measurements. Regardless, the measured data can be discussed. For all nine samples, the dynamic measurements are performed with a light and a medium seismic mass. Figure 6.1 shows an example of the displacement relative to the maximum deformation, it is shown at a frequency of 120 Hz, in Figure 6.2 the accompanying frequency response is shown. It can be seen that the samples do show anisotropic material deformation.

6.4 Static measurements results

As mentioned before, the moduli are not jet determined using inverse estimation. For all samples, the displacement fields in the principal directions are measured. An example of a result is shown in Figure 6.3. These results show asymmetric displacements which can result from anisotropy in the material.

Furthermore, a material discontinuity is visible in the results. At the edges of the sample, where it is fixed to the plates, the material shows a reduced stiffness. This phenomenon is also visible in the load measurements. In the first ten seconds of the compression the needed load to compress the material is lower, the slope is smaller. This is shown in Figure 6.4. This effect is also discussed in [6]; the cells at the edges of the foam might be damaged when cutting the sample.

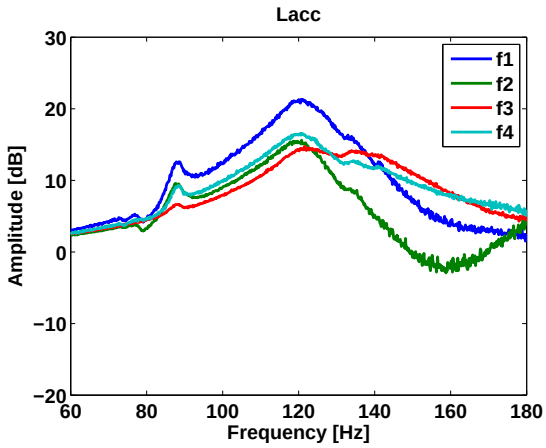

Figure 6.2: Frequency response plot of the four corners: f1, f2, f3, f4

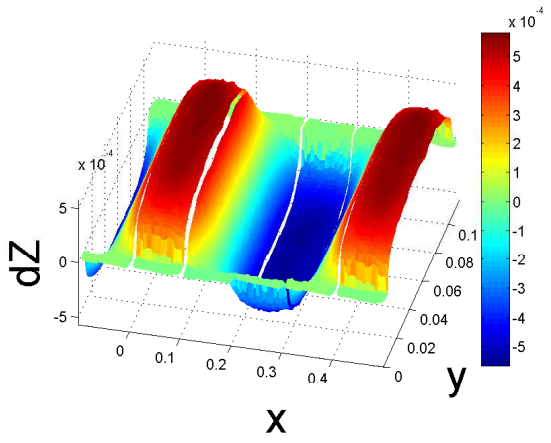

Figure 6.3: Measured deformation map of a sample, here the faces of the sample are matched with each other

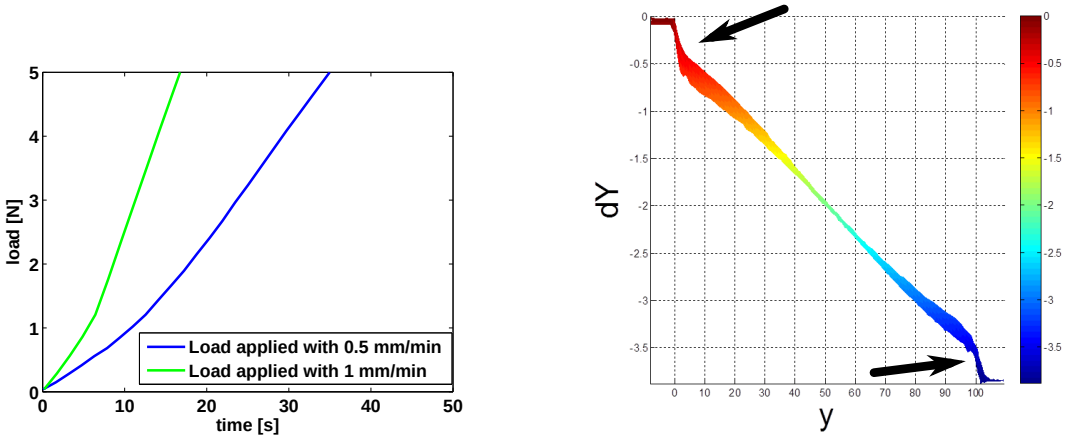

Figure 6.4: Material discontinuity at the boundary condition (reduced stiffness)

Chapter 7

Conclusions and recommendations

The goal of the internship was to do the measurements to gather new data, for modeling and performing simulations, and to improve them. Furthermore, the second goal was to write manuals for the measurements, such that measurements can be done for other materials and the same way as described in this report. All goals are accomplished.

The flow resistivity measurements showed similar results as previous results, like in [4]. From the results it can be concluded that the material show anisotropic behavior. Furthermore, it can be said that the rise direction of the foam is aligned with the z-coordinate.

For moduli it is expected that they are higher in the rise direction than in the plane normal to it [8]. But, the Hooke's tensor is not determined jet. All data is gathered but the inverse estimation is not jet applied. Regardless this, the data could be analyzed. The results from the dynamic measurements showed that the samples show anisotropic behavior when looking at the relative displacements and the frequency responses.

The displacement fields showed reduced stiffness at the edges. This might be caused by damaged cells at the edges. Furthermore, also in the displacement maps showed the anisotropy of the melamine foam.

For measuring flow resistivity, it is already possible to measure the property in all principle directions with one sample. This should improve the static and dynamic measurements, now three different sample are used for the principle directions. This makes the measurements more accurate because in the inverse estimation the assumption is made that these measurements are done with one sample instead of three.

Appendix A

Results of the flow resistivity measurements

Table A.1: Eigenvalue and eigenvector decomposition of measured resistivity per sample

sample	weight [g]	eigenvalues	eigenvectors		
1	9.2	6.193	0.9971	-0.0749	0.0129
		6.528	0.0746	0.9969	0.0262
		6.900	-0.0148	-0.0252	0.9996
2	9	6.130	0.7946	0.6026	0.0745
		6.255	0.6003	-0.7981	0.0522
		6.522	-0.0909	-0.0032	0.9959
3	9.1	6.520	0.8297	0.4923	0.2632
		6.733	0.5395	-0.8283	-0.1513
		7.183	-0.1435	-0.2675	0.9528
4	9.1	6.479	0.8063	0.5905	-0.0350
		6.607	-0.5805	0.8013	0.1446
		7.120	0.1135	-0.0963	0.9889
5	9	6.316	0.9974	-0.0273	0.0670
		6.518	0.0014	0.9330	0.3598
		6.810	-0.0723	-0.3587	0.9306
6	9.2	6.698	-0.1497	0.6874	0.7107
		6.742	0.9808	0.0122	0.1948
		7.033	-0.1253	-0.7262	0.6760
7	9.2	6.644	-0.1687	0.9616	-0.2166
		6.736	-0.9311	-0.0834	0.3551
		7.056	0.3234	0.2616	0.9094
8	9.2	6.185	0.2726	-0.9582	0.0864
		6.297	0.9467	0.2512	-0.2016
		6.763	0.1715	0.1367	0.9756
9	9.1	6.770	0.7286	0.5080	-0.4593
		6.939	0.5817	-0.8130	0.0236
		7.318	0.3615	0.2844	0.8880

Bibliography

[1] Iso 9053:1991: Acoustics - materials for acoustical applications - determination of airflow resistance. 1991.

[2] Basotect. Basf plasticsportal - foams , http://www.basotect.com, September 2013.

[3] J. Cuenca and P. Göransson. Inverse estimation of the elastic and anelastic properties of the porous frame of anisotropic open-cell foams. *The Journal of the Acoustical Society of America*, 132(2):621–629, 2012.

[4] C. Van der Kelen. Characterisation of anisotropic acoustic properties of porous materials - inverse estimation of static flow resistivity, 2011. Licenciate thesis.

[5] Lorna J. Gibson and Micheal F. Ashby. *Cellular solids: structure and properties.* Cambridge : Cambridge University Press, 1997.

[6] R. Guastavino. *Elastic and Acoustic Characterisation of Anisotropic Porous Materials.* PhD thesis, KTH, Stockholm, 2009.

[7] M. Abom H. Bodén H.P. Wallin, U. Carlsson and R. Glav. *Sound and Vibration.* Marcus Wallenberg Laboratoriet för Ljud- och Vibrationsforskning, 2012.

[8] A.T. Huber and L.J. Gibson. Anisotropy of foams. *Journal of Materials Science*, 23(8):3031–3040, 1988.

[9] GOM mbH. *ARAMIS v6.3 User Manual*, 2011.